



Texture and microstructure of Cr_2O_3 and $(\text{Cr,Al})_2\text{O}_3$ thin films deposited by reactive inductively coupled plasma magnetron sputtering

K. Pedersen^a, J. Bøttiger^a, M. Sridharan^{a,1}, M. Sillassen^a, P. Eklund^{a,b,*}

^a Interdisciplinary Nanoscience Center (iNANO) and Department of Physics and Astronomy, University of Aarhus, DK-8000 Aarhus C, Denmark

^b Thin Film Physics Division/FunMat, Dept. of Physics, Chemistry, and Biology (IFM), Linköping University, SE-581 83 Linköping, Sweden

ARTICLE INFO

Article history:

Received 15 August 2009

Received in revised form 8 December 2009

Accepted 7 January 2010

Available online 15 January 2010

Keywords:

Alumina

Chromia

Physical vapor deposition

Coatings

Preferred orientation

X-ray diffraction

ABSTRACT

Cr_2O_3 and $(\text{Cr,Al})_2\text{O}_3$ films were grown using reactive dc and inductively coupled plasma magnetron sputtering at substrate temperatures of 300–450 °C. For pure chromia, α - Cr_2O_3 films with fiber texture were grown; the out-of-plane texture could be controlled from $\langle 0001 \rangle$ to $\langle 10\bar{1}4 \rangle$. The former texture was obtained as a consequence of competitive growth with no applied bias or inductively coupled plasma, while the latter was obtained at moderate bias (−50 V), probably due to recrystallization driven by ion-bombardment-induced strain. By reactive codeposition of Cr and Al, a corundum-structured metastable solid solution α -($\text{Cr,Al})_2\text{O}_3$ with Cr/Al ratios of 2–10 was grown with a dense, fine-grained morphology. Hardness and reduced elastic modulus values were in the ranges 24–27 GPa and 190–230 GPa, respectively.

© 2010 Elsevier B.V. All rights reserved.

1. Introduction

Low-temperature physical vapor deposition (PVD) of crystalline Al_2O_3 (alumina), and especially the thermodynamically stable α phase, has been approached from two main directions. One is to use ionized PVD (I-PVD) techniques [1], an approach that has yielded low-temperature-deposited θ -, κ -, and γ -alumina films [2–7] with higher crystallinity than for conventional PVD, and has permitted growth of α - Al_2O_3 at temperatures below 700 °C [8–10]. The second approach is to promote the nucleation of α - Al_2O_3 either by a crystallographic template such as α - Cr_2O_3 [11–13] or in solid solution α -($\text{Cr,Al})_2\text{O}_3$ [14–17]. We have previously investigated [5,6] amorphous and γ -alumina thin films deposited by the I-PVD technique inductively coupled plasma magnetron sputtering (ICP-MS), which uses an rf coil to increase the degree of ionization in the deposition flux [18]. Subsequently, we employed chromia template layers and demonstrated that the texture of the template strongly influenced the nucleation of α - Al_2O_3 [13]. This background motivates the present work, where we have investigated the texture effects in pure chromia films and the deposition of α -($\text{Cr,Al})_2\text{O}_3$ thin films with and without chromia template layers, using dc magnetron sputtering and ICP-MS.

2. Experimental details

Cr_2O_3 and Cr–Al–O thin films were deposited by reactive dc magnetron sputtering and ICP-MS with 25-mm Cr (99.995%, operated in dc power control mode, 40 W unless stated otherwise) and Al (99.995%, operated in current control mode with pulsed dc) targets. Details can be found elsewhere [5,13]. Si(100) substrates (15 × 15 mm²) with native oxide were used. When a negative bias was applied to the substrate, an rf power supply was used (the bias voltages stated in this paper are the dc-equivalent voltages). The base pressure was lower than 10^{−5} Pa. The working pressure was 0.75–0.80 Pa with partial pressures of Ar (99.9996%) and O₂ (99.99990%) of 0.70 and 0.05–0.10 Pa, respectively (in flow-control mode). The substrate temperature was in the range from 300 °C to 450 °C. The target-to-substrate distances were ~100 mm. Fig. 1 is a schematic drawing of the deposition geometry. For the codeposition experiments, the angle between the substrate holder axis and the Cr and Al targets is ~30°, with the magnetrons on either side. However, the angle χ defined in Fig. 1 (i.e., the angle between the Cr target and the substrate holder) can be chosen in the full range 0–360° by positioning the substrate holder, e.g., the substrate holder can be tilted so that it faces either target. Note that the substrate position in the substrate holder is somewhat above the axis of the substrate holder. The angle χ is therefore not the same as the incidence angle of the deposition flux, like it is in a glancing angle deposition setup [19].

X-ray diffraction (XRD) θ – 2θ measurements were carried out in a Bruker D8 diffractometer using CuK α radiation. Measurements in

* Corresponding author. Thin Film Physics Division/FunMat, Dept. of Physics, Chemistry, and Biology (IFM), Linköping University, SE-581 83 Linköping, Sweden.

E-mail address: perek@ifm.liu.se (P. Eklund).

¹ Present address: Center for Nanotechnology and Advanced Biomaterials (CeNTAB), SASTRA University, Thanjavur – 613 401, Tamil Nadu, India.

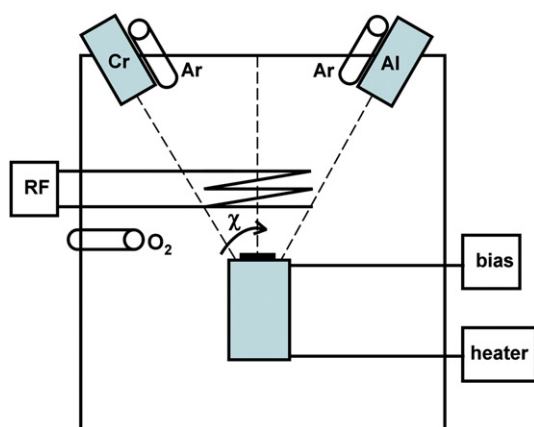


Fig. 1. Schematic drawing of the deposition geometry. The angle χ between the Cr target and the substrate holder can be chosen in the full range $0\text{--}360^\circ$ by positioning the substrate holder. $\chi=0^\circ$ when the substrate holder is directly facing the Cr target.

grazing incidence geometry ($2\text{--}10^\circ$ incidence) were also performed for all samples, but did not yield additional information and are therefore not included here. Scanning electron microscopy (SEM) images were acquired in a FEI NOVA 600 SEM with accelerating voltage 5 kV and working distance 5 mm. The elemental compositions of the films were measured by Rutherford backscattering spectroscopy (RBS) using 2-MeV $^4\text{He}^+$ ions and a scattering angle of 161° . The RBS spectra were simulated using the SIMNRA software [20].

Nanoindentation measurements were performed using a Tribo-Indenter (Hysitron Inc.) with a Berkovich tip. The hardness, H , and reduced elastic modulus, E_r , were determined according to the Oliver–Pharr procedure. 100 indents in the load range 3–10 mN (giving depth-independent H and E_r values) were made for each sample.

3. Results and discussion

3.1. Initial observations

During all depositions, the Ar flow was set at 5 sccm, corresponding to a partial pressure of 0.7 Pa (5 mTorr). The hysteresis effect was investigated by running the Cr target at 40 W dc power, varying the O_2 flow from 0 to 4 sccm and back (graphs not shown). When the rf coil was not used, metallic-mode sputtering occurred in the range 0–1 sccm, after which the expected transition region from metallic- to poisoned-mode sputtering was observed. At O_2 flows above 1.4 sccm, the target was in poisoned mode. No arcing was observed even in poisoned mode. When decreasing the O_2 flow, the target remained poisoned until ~ 0.5 sccm. When the rf coil was applied (coil power 100–200 W), the onset of the transition region was delayed until an O_2 flow of 1.1–1.2 sccm, and the transition region to poisoned mode was very narrow (the target was essentially poisoned at 1.3 sccm). This effect is expected given the increased ion bombardment on the target [21,22]. When decreasing the O_2 flow, the target remained poisoned until ~ 0.5 sccm, i.e., the same value as when the rf coil was not used. Regardless of whether the rf coil was used or not, the composition (determined by RBS) of films deposited in metallic mode did not differ significantly between 0.5 and 1 sccm O_2 flow. In this range, a composition of $\text{Cr}:\text{O} = 2:3$ (within the RBS error bars) and a stable sputtering process was obtained. Lower O_2 flow yielded films with understoichiometric CrO_x and/or metallic Cr, as expected [23–25]. Based on these results, the O_2 flow was fixed to 0.5 sccm for all remaining Cr_2O_3 depositions.

Fig. 2 shows cross-section SEM images of Cr_2O_3 films deposited without bias and rf coil at a substrate temperature of 300°C , with $\chi=30^\circ$ (Fig. 2a) and $\chi=0^\circ$ (Fig. 2b). The film deposited at $\chi=30^\circ$

has a tilted columnar structure, with the columns tilted 26° off-normal towards the deposition direction. In the film deposited at $\chi=0^\circ$, the columns are more or less orthogonal to the surface. Films deposited at higher target-substrate angles ($60\text{--}80^\circ$, not shown) also exhibited a tilted columnar morphology, but were thinner (~ 660 nm for 60° and ~ 175 nm for 80°) and underdense, as expected due to shadowing effects. Films deposited at higher temperature (450°C) exhibited the same phenomenon of tilted growth but with a lower column-tilt angle (e.g., $\sim 14^\circ$ off-normal for films deposited at an angle between target and substrate holder of 30°). In contrast, films deposited using the rf coil exhibited only columnar growth with the columns orthogonal to the surface (not shown, very similar to Fig. 2b), irrespective of rf-coil power and bias.

The tilting effect is expected at the kinetically limited conditions at $300\text{--}450^\circ\text{C}$. The higher temperature gives reduced tilting effect compared to the lower temperature because of the increased diffusivity at higher temperature [19]. In contrast, a partially ionized flux of energetic Cr (and any Cr–O species) means that adatoms arriving at the surface of the growing film have a high diffusivity and column tilting is avoided.

For all remaining Cr_2O_3 deposition experiments at floating potential without rf coil, the angle χ was thus set to 0, i.e., the substrate was directly facing the target in order to avoid column tilting. For samples deposited using the rf coil, no difference was observed for $\chi=0^\circ$ and $\chi=30^\circ$, and the results are equivalent.

3.2. Texture effects in chromia films

In all cases, the film thickness (as measured by cross-section SEM and corroborated by RBS) scaled nearly, but not fully, linearly with the deposition time. A deposition time of 15 min corresponds to ~ 125 nm, 30 min to ~ 225 nm, 45 min to 400–440 nm, and 60 min to 500–550 nm film thickness.

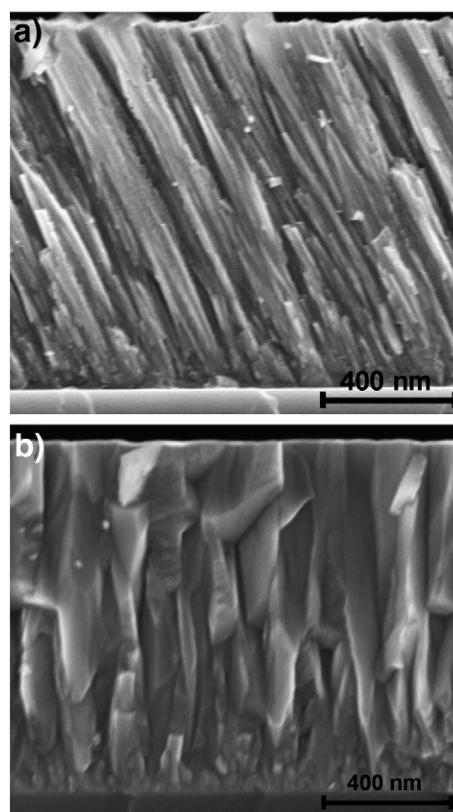


Fig. 2. Cross-section SEM images of Cr_2O_3 films deposited without bias and rf coil at a substrate temperature of 300°C , with $\chi=30^\circ$ (a) and $\chi=0^\circ$ (b).

Fig. 3 shows θ - 2θ X-ray diffractograms of Cr_2O_3 films deposited at 450 °C and floating potential (no bias or rf coil) for (a) 15 min, (b) 30 min, (c) 45 min, and (d) 60 min. The films deposited for 15–30 min (Fig. 3(a) and (b)) exhibit a strong 0006 peak with no other peaks observed; for thicker films (Fig. 3(c) and (d)) an additional 01 $\bar{1}$ 2 peak (and its 02 $\bar{2}$ 4 multiple) is present, while the 0006 peak remains dominant. These results show that these films have a pure $\langle 0001 \rangle$ texture (out-of-plane), or for thicker films, a dominant $\langle 0001 \rangle$ texture with a $\langle 01\bar{1}2 \rangle$ component. In comparison, the intensity ratio between the 01 $\bar{1}$ 2 and 0006 peaks is ~ 10 for randomly oriented polycrystalline Cr_2O_3 [ICDD PDF 38-1479]. Fig. 4 shows θ - 2θ X-ray diffractograms of Cr_2O_3 films deposited at 450 °C, –50 V bias, and 150 W rf-coil power for (a) 15 min, (b) 30 min, (c) 45 min, and (d) 60 min. All these films exhibit a strong $\langle 10\bar{1}4 \rangle$ texture with a small $\langle 11\bar{2}6 \rangle$ component. The peaks are relatively broad (full width at half maximum of $\sim 1.2^\circ 2\theta$) and somewhat asymmetric, indicating a high level of microstrain and/or a small size of the coherently diffracting domains. This observation suggests that many stacking faults and other defects are caused by the ion bombardment during growth. For all films, the texture is a fiber texture as evidence by pole figure plots (not shown, cf., fig. 1 in Ref. [13]). Fig. 5 shows θ - 2θ X-ray diffractograms of Cr_2O_3 films deposited at 300 °C, –50 V bias, and 150 W rf-coil power for (a) 15 min, (b) 30 min, (c) 45 min, and (d) 60 min. The thicker films (Fig. 5(c) and (d)) exhibit the same strong $\langle 10\bar{1}4 \rangle$ texture with a small $\langle 11\bar{2}6 \rangle$ component as in Fig. 4. However, the thinner films (≤ 250 nm) exhibit three small peaks at 2θ positions of 39.1°, 44.0°, and 48.5°. The two lower peaks correspond to the 0006 and 20 $\bar{2}$ 2 peaks of Cr_2O_3 ; however, the third peak is not a match to Cr_2O_3 . Possibly, these samples include a small amount of the suboxide Cr_3O which would match these three peak positions, although systematically shifted to lower angles compared to their equilibrium positions [ICDD PDF 72-0528]. Note that the films are stoichiometric (i.e., 2Cr:3O within the RBS error bars, with no other elements detected). These peaks may therefore be due to a combination of Cr_2O_3 and a small amount of Cr_3O with an overall composition relatively close to 2Cr:3O. The peaks are shifted by $\sim 0.5^\circ$ to lower angles compared to their equilibrium positions (equivalent to an increase in out-of-plane lattice spacing of $\sim 1.5\%$), indicating a high level of in-plane compressive strain.

The $\langle 0001 \rangle$ texture observed in Fig. 3 is expected as a consequence of competitive growth [26,27]. The difference in texture between Figs. 4 and 5 is more likely caused by a strain-driven recrystallization mechanism. The mixed texture observed in Fig. 5 at low film thickness, with peaks shifted to lower angles compared to their equilibrium positions, indicates a high level of in-plane compressive (macroscopic) strain. Therefore, the shift to a $\langle 10\bar{1}4 \rangle$

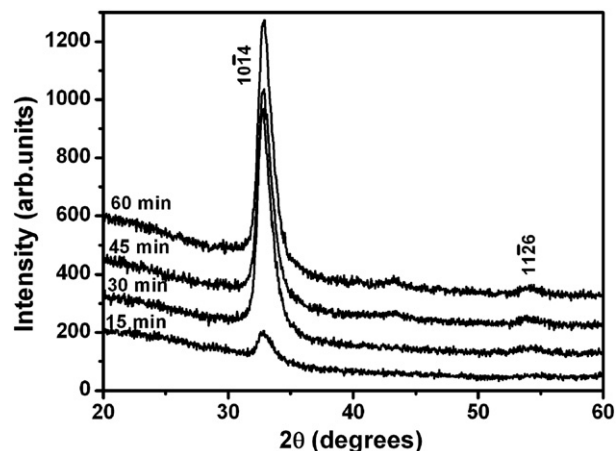


Fig. 4. θ - 2θ X-ray diffractograms of Cr_2O_3 films deposited at 300 °C, –50 V bias, and 150 W rf-coil power for (a) 15 min, (b) 30 min, (c) 45 min, and (d) 60 min.

texture for thicker films can be attributed to strain-driven recrystallization, i.e., a new set of $\langle 10\bar{1}4 \rangle$ -oriented grains grow at the expense of the highly strained grains with mixed orientation. This type of recrystallization mechanism due to ion-bombardment-induced lattice defects and corresponding strain has been explained by Dong and Srolovitz [28]. A recrystallization mechanism would also explain the difference between Figs. 4 and 5, in that the driving force for recrystallization is a combination of temperature and strain. Therefore, for lower temperature (300 °C), the films are required to grow to a much higher thickness (> 250 nm) before the driving force for recrystallization is sufficient, while at higher temperature (450 °C), recrystallization would occur for much thinner films and therefore not be observed in Fig. 4, where the lowest film thickness is ~ 125 nm (15 min deposition time).

Films deposited at –50 V bias exhibited very similar results regardless of rf-coil power (100–200 W); the results for an rf-coil power of 150 W described above are representative for all samples. Films deposited at higher bias (–100 V or –150 V) differed, however. Fig. 6 shows the XRD pattern of a representative Cr_2O_3 film deposited at higher bias (–100 V bias and 150 W rf-coil power). Several broad, low-intensity peaks can be observed, indicating small α - Cr_2O_3 grain sizes with relatively (but not fully) random texture of the grains. XSEM (not shown) showed a morphology consistent with a fine-grained polycrystalline structure. These results indicate that the high ion bombardment results in a small grain size with relatively random crystallite orientation, as expected [26,27,29–31] due to the

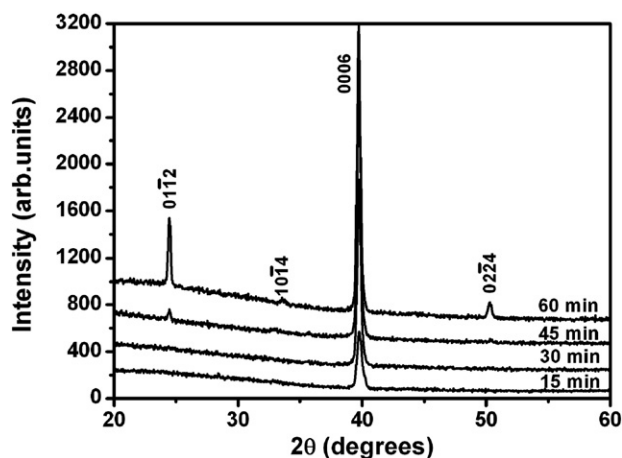


Fig. 3. θ - 2θ X-ray diffractograms of Cr_2O_3 films deposited at 450 °C and floating potential for (a) 15 min, (b) 30 min, (c) 45 min, and (d) 60 min.

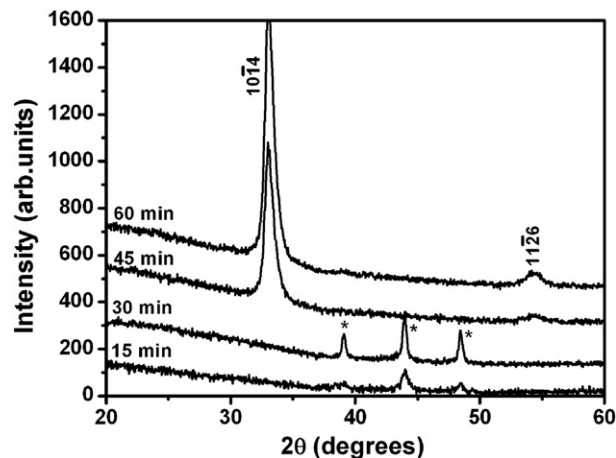


Fig. 5. θ - 2θ X-ray diffractograms of Cr_2O_3 films deposited at 450 °C, –50 V bias, and 150 W rf-coil power for (a) 15 min, (b) 30 min, (c) 45 min, and (d) 60 min.

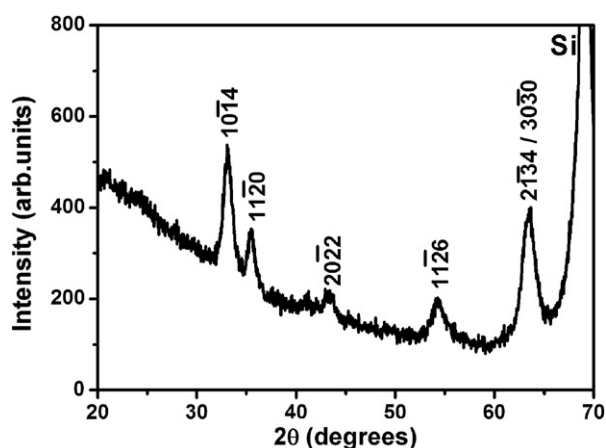


Fig. 6. θ – 2θ X-ray diffractograms of Cr_2O_3 film deposited at 450 °C, –100 V bias, and 150 W rf-coil power for 60 min (film thickness ~500 nm).

formation – by ion bombardment – of more nucleation centers giving a high nucleation rate of new grains and inducing a more random orientation.

Finally, we note that the O_2 flow has been a fixed parameter in this investigation. However, it is known that the amount of O_2 will affect the adatom diffusivities [27] and is therefore in general also likely to affect the texture of the films [23].

In summary, the fiber texture of the chromia films could be controlled from a $\langle 0001 \rangle$ texture, due to competitive growth, to a $\langle 10\bar{1}4 \rangle$ texture, probably due to recrystallization driven by ion-bombardment-induced strain. The $\langle 10\bar{1}4 \rangle$ -textured chromia films apparently have a large number of stacking faults and other defects as indicated by the asymmetric peak broadening. This observation is likely relevant to our previous observation that α -alumina nucleation occurred more easily on the $\langle 10\bar{1}4 \rangle$ -textured Cr_2O_3 templates than on the $\langle 0001 \rangle$ -textured ones. Both the introduction of a large number of point defects that act as preferential nucleation sites on the chromia surface and surface cleaning by ion bombardment to reduce the amount of adsorbed impurities (especially hydrogen [32–35]) are likely to facilitate the nucleation of $\alpha\text{-Al}_2\text{O}_3$.

3.3. Deposition of $\alpha\text{-(Cr,Al)}_2\text{O}_3$

A hysteresis investigation similar to the one described above for pure chromia was performed for the reactive codeposition of Cr–Al–O. The results were very similar except that the range (O_2 flow of 0.8–0.9 sccm) in which metallic-mode sputtering with stoichiometric oxide films (as determined by RBS) was obtained was much narrower than for pure chromia. The O_2 flow was therefore set at 0.8 sccm for all Cr–Al–O depositions. Two series of Cr–Al–O thin films were deposited; one series onto $\langle 10\bar{1}4 \rangle$ -textured chromia layers (deposited for 60 min, identical to Fig. 4(d)) and one series where Al and Cr were co-deposited throughout the entire deposition. In all depositions, the Cr target power was fixed; the Al target current was varied (425 mA, 450 mA, 475 mA, 520 mA).

One important difference was observed between the two series (with and without chromia prelayers). The films without chromia prelayers were very rough, evident already to the naked eye: they exhibited a gray, milky appearance indicative of the scattering of light at a rough surface. The higher the Al content, the more evident the roughness was. Therefore, both the RBS and the nanoindentation measurements yielded erratic results for these samples. In contrast, the films deposited onto chromia prelayers were smooth and yielded consistent, reliable RBS and nanoindentation data. The reason for this

striking difference in roughness is not known. For this reason, we focus on the films deposited onto chromia prelayers.

Fig. 7 shows XRD patterns from Cr–Al–O films deposited onto $\langle 10\bar{1}4 \rangle$ -textured Cr_2O_3 prelayers for varying Al content. All peaks can be assigned to a corundum-structured solid solution $\alpha\text{-(Cr,Al)}_2\text{O}_3$. For the lowest Al content, the peak positions are very close to those of pure $\alpha\text{-Cr}_2\text{O}_3$ [ICDD PDF 38-1479]. For decreasing Cr/Al ratio, all peaks shift systematically to higher 2θ angles, towards the positions for $\alpha\text{-Al}_2\text{O}_3$ [ICDD PDF 46-1212]. This systematic reduction in lattice parameters with increasing Al content is consistent with the solid solution $\alpha\text{-(Cr,Al)}_2\text{O}_3$. The broad peak at 64.3° is a combination of the overlapping 2134 and 3000 peaks. The results strongly indicate the formation of a solid solution $\alpha\text{-(Cr,Al)}_2\text{O}_3$, which is expected according to the phase diagram [36] at Cr/Al ratios higher than ~4; however, the samples with Cr/Al=2 are well into the miscibility gap and here, the $\alpha\text{-(Cr,Al)}_2\text{O}_3$ is thus a metastable solid solution.

Fig. 8 shows cross-section SEM images of the samples deposited onto chromia prelayers, with Cr/Al ratios of ~4 (Fig. 8a) and ~2 (Fig. 8b). Samples with lower Al content (Cr/Al ratio of 8–10, not shown) were very similar in morphology to the sample with Cr/Al ~4. For low Al content (Cr/Al ratios of 4–10), the columnar morphology of the chromia prelayer is retained throughout the film; however, the individual columns are not single crystals as in the chromia layer. Instead, the individual columns contain smaller crystallites of increasingly random, but not fully random, orientation, as evidenced by XRD. For high Al content, the morphology of the chromia layer is not retained; instead, a dense, fine-grained morphology of $\alpha\text{-(Cr,Al)}_2\text{O}_3$ grains is obtained. This is somewhat surprising given that pure $\alpha\text{-Al}_2\text{O}_3$ readily grows onto these templates, and the individual $\alpha\text{-Al}_2\text{O}_3$ columns are relatively large single crystals (cf., Ref. [13]). Possibly, the reactive codeposition of Cr and Al yields reduced mobilities compared to the binary oxides, resulting in a fine-grained structure and facilitating the formation of an $\alpha\text{-(Cr,Al)}_2\text{O}_3$ solid solution rather than a phase separation into Cr_2O_3 and Al_2O_3 . This argument is supported by the clear indications in the literature [33,37] that limited adatom mobilities are not one of the main limitations for growth of pure $\alpha\text{-Al}_2\text{O}_3$ growth in this temperature range; therefore, the formation of a corundum-structure solid solution should not be impeded by a reduction in surface mobilities.

The hardness values for all the $\alpha\text{-(Cr,Al)}_2\text{O}_3$ films are in the range 24–27 GPa, somewhat lower than that of the pure chromia films (29 GPa) [13], and the reduced elastic moduli were measured to be in the range 190–230 GPa.

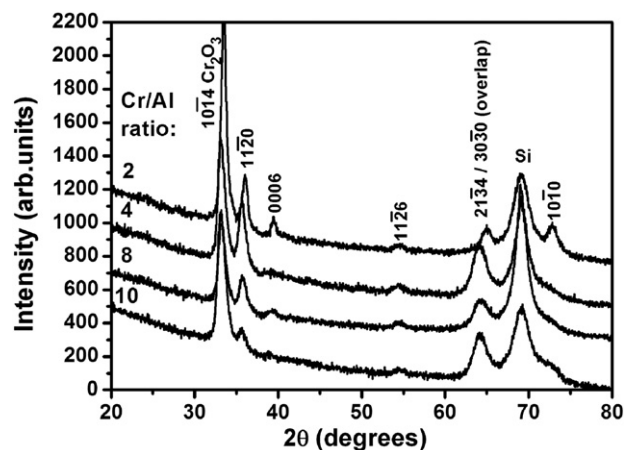


Fig. 7. θ – 2θ X-ray diffractograms of $(\text{Cr,Al})_2\text{O}_3$ thin films with varying Al content (Cr/Al ratios of ~2, ~4, ~8, and ~10) deposited onto $\langle 10\bar{1}4 \rangle$ -textured chromia prelayers.

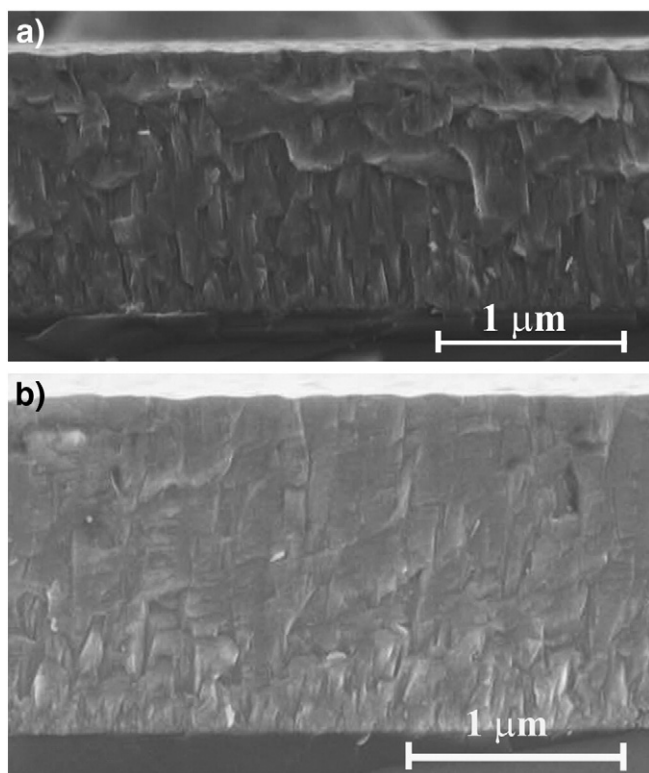


Fig. 8. Cross-section SEM images of $(\text{Cr,Al})_2\text{O}_3$ thin films with Cr/Al ratios of (a) ~ 4 and (b) ~ 2 , deposited onto $\langle 10\bar{1}4 \rangle$ -textured chromia prelayers.

4. Concluding remarks

Chromia films with fiber texture were grown; the out-of-plane texture could be controlled from a $\langle 0001 \rangle$ texture, due to competitive growth, to a $\langle 10\bar{1}4 \rangle$ texture, probably due to recrystallization driven by ion-bombardment-induced strain. The latter films apparently have a large number of stacking faults and other defects as indicated by the asymmetric peak broadening. This is relevant for the use of chromia templates to promote α -alumina nucleation. Both the introduction of a large number of point defects that act as preferential nucleation sites on the chromia surface and surface cleaning by ion bombardment to reduce the amount of adsorbed impurities are likely to facilitate the nucleation of α - Al_2O_3 . It is difficult to account for these effects in theoretical studies of α - Al_2O_3 nucleation onto α - Cr_2O_3 [38–41]; however, the effect of impurities has been theoretically investigated for pure Al_2O_3 [33,34] and there is a need for similar studies for the $\text{Cr}_2\text{O}_3/\text{Al}_2\text{O}_3$ system.

For Cr–Al–O films, a corundum-structured solid solution α -(Cr, Al) $_2\text{O}_3$ with Cr/Al ratios of 2–10 was grown with a dense, fine-grained morphology. The lowest Cr/Al ratio is well into the miscibility gap, i.e., the α -(Cr, Al) $_2\text{O}_3$ is a metastable solid solution. The hardness was in the range 24–27 GPa, somewhat lower than that of the pure chromia films (29 GPa).

Contributors

This paper is based mainly on K. Pedersen's M. Sc. Thesis, for which P. Eklund served as supervisor. K. P. performed the majority of the deposition experiments, XRD and SEM analysis and interpretation. P. E. also contributed to planning, analysis, and interpretation, deposition experiments, and wrote the paper based on K.P.'s thesis. J. Böttiger served as examiner and contributed to planning and

interpretation. M. Sridharan contributed to the design, planning, and setup of the experiments. M. Sillassen performed the RBS measurements and analyzed and interpreted the RBS data. All coauthors read and commented on the manuscript.

Acknowledgments

Funding from the Danish NABIIT program is acknowledged. P. E. acknowledges support from the Carlsberg Foundation and the Swedish Agency for Innovation Systems (VINNOVA) VINN Excellence Center in Research & Innovation on Functional Nanostructured Materials (FunMat).

References

- [1] U. Helmersson, M. Lattemann, J. Bohlmark, A.P. Ehiassarian, J.T. Gudmundsson, *Thin Solid Films* 513 (2006) 1.
- [2] J.M. Schneider, W.D. Sproul, A.A. Voevodin, A. Matthews, *J. Vac. Sci. Technol. A* 5 (1997) 1084.
- [3] J.M. Schneider, W.D. Sproul, A. Matthews, *Surf. Coat. Technol.* 98 (1997) 1473.
- [4] A. Khanna, D.G. Bhat, *Surf. Coat. Technol.* 201 (2006) 168.
- [5] M. Sridharan, M. Sillassen, J. Böttiger, J. Chevallier, H. Birkedal, *Surf. Coat. Technol.* 202 (2007) 920.
- [6] P. Eklund, M. Sridharan, G. Singh, J. Böttiger, *Plasma Process. Polym.* 6 (2009) S907.
- [7] V. Edlmayr, M. Moser, C. Walter, C. Mitterer, *Surf. Coat. Technol.* 204 (2010) 1576.
- [8] E. Wallin, T.I. Selinder, M. Elfving, U. Helmersson, *Europhys. Lett.* 82 (2008) 36,002.
- [9] T.I. Selinder, E. Coronel, E. Wallin, U. Helmersson, *Int. J. Refract. Met. Hard Mat.* 27 (2009) 507.
- [10] K. Sarakinos, J. Alami, S. Konstantinidis, *Surf. Coat. Technol.* 204 (2010) 1661.
- [11] P. Jin, G. Xu, M. Tazawa, K. Yoshimura, D. Music, J. Alami, U. Helmersson, *J. Vac. Sci. Technol. A* 20 (2002) 2134.
- [12] J.M. Andersson, Z.S. Czizgany, P. Jin, U. Helmersson, *J. Vac. Sci. Technol. A* 22 (2004) 117.
- [13] P. Eklund, M. Sridharan, M. Sillassen, J. Böttiger, *Thin Solid Films* 516 (2008) 7447.
- [14] M. Witthaut, R. Cremer, K. Reichert, D. Neuschütz, *Mikrochim. Acta* 133 (2000) 191.
- [15] J. Ramm, M. Ante, T. Bachmann, B. Widrig, H. Brändle, M. Döbeli, *Surf. Coat. Technol.* 202 (2007) 876.
- [16] J. Ramm, M. Ante, H. Brändle, A. Neels, A. Dommann, M. Döbeli, *Adv. Eng. Mater.* 9 (2007) 604.
- [17] D.E. Ashenford, F. Long, W.E. Hagston, B. Lunn, A. Matthews, *Surf. Coat. Technol.* 116–119 (1999) 699.
- [18] S.M. Rosnagel, J. Hopwood, *J. Vac. Sci. Technol. B* 12 (1994) 449.
- [19] M.M. Hawkeye, M.J. Brett, *J. Vac. Sci. Technol. A* 25 (2007) 1317.
- [20] M. Mayer, *Nucl. Instr. Meth. B* 194 (2002) 177.
- [21] S. Konstantinidis, C. Nouvellon, J.-P. Dauchot, M. Wautelet, M. Hecq, *Surf. Coat. Technol.* 174–175 (2003) 100.
- [22] R. Snyders, J.-P. Dauchot, M. Hecq, *Plasma Process. Polym.* 4 (2007) 113.
- [23] G. Contoux, F. Cosset, A. Célérier, J. Machet, *Thin Solid Films* 292 (1997) 75.
- [24] P. Hones, M. Diserens, F. Lévy, *Surf. Coat. Technol.* 120–121 (1999) 277.
- [25] P. Eklund, N.-J. Mikkelsen, M. Sillassen, E.J. Bieck, J. Böttiger, *Surf. Coat. Technol.* 203 (2008) 156.
- [26] G. Abadias, *Surf. Coat. Technol.* 202 (2008) 2223.
- [27] I. Petrov, P.B. Barna, L. Hultman, J.E. Greene, *J. Vac. Sci. Technol. A* 21 (2003) S117.
- [28] L. Dong, D.J. Srolovitz, *Appl. Phys. Lett.* 75 (1999) 584.
- [29] M. Tabbal, S. Kahwaji, T.C. Christidis, B. Nsouli, K. Zahraman, *Thin Solid Films* 515 (2006) 1976.
- [30] M. Sillassen, P. Eklund, M. Sridharan, N. Pryds, N. Bonanos, J. Böttiger, *J. Appl. Phys.* 105 (2009) 104,907.
- [31] D.-Y. Wang, J.-H. Lin, W.-Y. Ho, *Thin Solid Films* 332 (1998) 295.
- [32] J. Rosén, E. Widenkvist, K. Larsson, U. Kreissig, S. Mráz, C. Martinez, D. Music, J.M. Schneider, *Appl. Phys. Lett.* 88 (2006) 191,905.
- [33] J. Rosén, K. Larsson, J.M. Schneider, *J. Phys., Condens. Matter* 17 (2005) L137.
- [34] E. Wallin, J.M. Andersson, E.P. Mürger, V. Chirita, U. Helmersson, *Phys. Rev. B* 74 (2006) 125,409.
- [35] E. Wallin, J.M. Andersson, M. Lattemann, U. Helmersson, *Thin Solid Films* 516 (2008) 3877.
- [36] M. Fujita, K. Inukai, S. Sakida, T. Nanba, J. Ommyoji, A. Yamaguchi, Y. Miura, *J. Soc. Mater. Sci. Jpn* 56 (2007) 526.
- [37] E. Wallin, E.P. Mürger, V. Chirita, U. Helmersson, *J. Phys. D: Appl. Phys.* 42 (2009) 125,302.
- [38] J. Sun, T. Stirner, A. Matthews, *Surf. Coat. Technol.* 201 (2006) 4205.
- [39] J. Sun, T. Stirner, A. Matthews, *Surf. Sci.* 601 (2007) 5050.
- [40] J. Sun, T. Stirner, A. Matthews, *Surf. Sci.* 601 (2007) 1358.
- [41] J. Sun, T. Stirner, *Thin Solid Films* 517 (2009) 5512.